

Mutations of evolutionarily conserved aromatic residues suggest that misfolding of the mouse prion protein may commence in multiple ways

Suman Pal  | Jayant B. Udgaonkar

Indian Institute of Science Education and Research Pune, Pune, India

Correspondence

Jayant B. Udgaonkar, Indian Institute of Science Education and Research Pune, Pune 411008, India.
Email: jayant@iiserpune.ac.in; jayant@ncbs.res.in

Funding information

Department of Biotechnology, Government of India; Indian Institute of Science Education and Research Pune; J C Bose National Fellowship, Government of India

Abstract

The misfolding of the mammalian prion protein from its α -helix rich cellular isoform to its β -sheet rich infectious isoform is associated with several neurodegenerative diseases. The determination of the structural mechanism by which misfolding commences, still remains an unsolved problem. In the current study, native-state hydrogen exchange coupled with mass spectrometry has revealed that the N state of the mouse prion protein (moPrP) at pH4 is in dynamic equilibrium with multiple partially unfolded forms (PUFs) capable of initiating misfolding. Mutation of three evolutionarily conserved aromatic residues, Tyr168, Phe174, and Tyr217 present at the interface of the β 2- α 2 loop and the C-terminal end of α 3 in the structured C-terminal domain of moPrP significantly destabilize the native state (N) of the protein. They also reduce the free energy differences between the N state and two PUFs identified as PUF1 and PUF2^{**}. It is shown that PUF2^{**} in which the β 2- α 2 loop and the C-terminal end of α 3 are disordered, has the same stability as the previously identified PUF2^{*}, but to have a very different structure. Misfolding can commence from both PUF1 and PUF2^{**}, as it can from PUF2^{*}. Hence, misfolding can commence and proceed in multiple ways from structurally distinct precursor conformations. The increased extents to which PUF1 and PUF2^{**} are populated at equilibrium in the case of the mutant variants, greatly accelerate their misfolding. The results suggest that the three aromatic residues may have been evolutionarily selected to impede the misfolding of moPrP.

KEYWORDS

aromatic residues, hydrogen-exchange, mass-spectrometry, mouse prion protein, partially unfolded form, prion misfolding

1 | INTRODUCTION

Prion diseases, also known as transmissible spongiform encephalopathies, constitute a group of fatal neurodegenerative diseases, characterized by the accumulation of the misfolded isoform (PrP^{Sc}) of the mammalian prion protein, in the central nervous system

(Kretzschmar et al., 1986; Moore et al., 2009). The mature cellular isoform (PrP^C) of the mouse prion protein (moPrP) is 208 amino acid residues long, and consists of two distinct domains: an intrinsically disordered N-terminal domain (NTD) and a structured C-terminal globular domain (CTD; Riek et al., 1996). The NTD has a 5-octarepeat region, which can bind metal ions, and is thought to be important

Abbreviations: CD, circular dichroism; CTD, C-terminal domain; HDX-MS, hydrogen-deuterium exchange coupled with mass-spectrometry; moPrP, mouse prion protein; PUF, partially unfolded form; wt, wild type.

in prion aggregation (Burns et al., 2002; Moore et al., 2006). The NTD also contains a hydrophobic stretch of highly conserved residues (Coleman et al., 2014), which play an important role in PrP^{Sc} interacting with the lipid membrane (Hegde et al., 1998). The structured CTD consists of three α -helices (α 1, α 2, and α 3), as well as a β -sheet consisting of two small anti-parallel β -strands (β 1 and β 2) (Riek et al., 1996). α 2 and α 3 are linked by a disulfide bond between Cys178 and Cys213 (mouse numbering is used throughout), which has been shown to be important in maintaining the stability of the protein (Ning et al., 2014).

The exact biological role of the prion protein in mammals is still unclear. The prion protein appears to play a role in several processes, including metal ion homeostasis (Rana et al., 2009; Vassallo & Herms, 2003; Watt & Hooper, 2003), cell signaling (Collinge et al., 1994; Haigh et al., 2010; Legname, 2017), cell adhesion (Málaga-Trillo et al., 2009; Martins et al., 2002; Schmitt-Ulms et al., 2001), and protection against oxidative stress (Brown, 2006; Choi et al., 2007; Milhavel & Lehmann, 2002; Wong et al., 2001). Transgenic mice in which the *Prnp* gene (*Prnp*^{0/0}) is knocked out, show sleep disturbance, altered circadian rhythms (Gasperini & Legname, 2014), as well as age-related cognitive decline (Steele et al., 2007). However, the mice were able to survive (Büeler et al., 1992), suggesting that the mammalian prion protein might have redundant functions, and not be an essential protein.

The susceptibilities of various mammals to sporadic prion diseases correlate well with the propensity of their PrP^C to misfold into β -sheet rich oligomers at low pH (Khan et al., 2010). In vivo, during its trafficking through the endocytic pathway, PrP^C enters lysosomes where it encounters a low pH (Borchelt et al., 1992). In vitro studies have shown that moPrP undergoes substantial structural fluctuations at acidic pH upon protonation of a critical residue, His186 (Singh & Udgaonkar, 2016a; Van der Kamp & Daggett, 2010), which facilitate oligomer formation. It is therefore likely that the prion protein misfolds into its oligomeric form when it encounters the low pH in the lysosome. At neutral pH, oligomerization cannot be studied, as only a negligibly small fraction of moPrP molecules have His.

One hundred and eighty-six in the protonated form (Singh & Udgaonkar, 2016a). Importantly, oligomers formed in vitro at low pH are cytotoxic (Erlich et al., 2010; Huang et al., 2010; Simoneau et al., 2007). They are able to disrupt lipid membranes (Caughey et al., 2009; Chich et al., 2010; Singh et al., 2014), which suggests a possible mechanism of their toxicity. Remarkably, a diseased human brain has recently yielded highly infectious small non-fibrillar oligomeric prion assemblies (Vanni et al., 2020). A better understanding of the disease as well as the development of therapeutic strategies against prion diseases will arise from knowledge of the misfolding of the prion protein that results in oligomerization.

The structures of the different mammalian prion proteins have been conserved during evolution, and the prion protein sequences show a high degree of amino acid similarity (Baiardi et al., 2019; Bernardi & Bruni, 2019). Regions that display sequence and structural

variation across different species include the β 2- α 2 loop and the C-terminal end of α 3, which are packed against each other (Bernardi & Bruni, 2019; Biljan et al., 2017; Slapšak et al., 2019). Three aromatic residues (Tyr168, Phe174, and Tyr217) present at the packing interface (Figure 1) are, however, highly conserved (Bartz et al., 1994; Huang & Caffisch, 2015; Kurt, Jiang, et al., 2014; van Rheede et al., 2003). Tyr168 and Tyr217 are strictly conserved, whereas Phe174 is conserved in all but two species (Huang & Caffisch, 2015). The aromatic interactions between Tyr168, Phe174, and Tyr217 are the most conserved aromatic interactions observed in the structures of different mammalian prion proteins (Zhang, 2015). MD simulation studies have suggested that favorable interactions between Tyr168, Phe174, and Tyr217 stabilize the interface of the β 2- α 2 loop and the C-terminal end of α 3 (Huang & Caffisch, 2015; Jung Cheng & Daggett, 2014). It is likely that the highly conserved aromatic residues play an important role in maintaining the integrity of the PrP^C structure and in guarding against misfolding that leads to the formation of oligomers.

In the current study, it is shown by mutational studies, that the evolutionarily conserved aromatic residues, Tyr168, Phe174, and Tyr217 indeed play a significant role in maintaining the structural integrity of the protein. The native (N) state of moPrP becomes unstable when the conserved aromatic residues are mutated to alanines, which also dramatically accelerates (up to 300-fold) the misfolding process. Native state hydrogen exchange (HDX) studies coupled with mass spectrometry (MS) have identified an aggregation-competent partially unfolded form (PUF2**), which is in rapid equilibrium with the N state at pH4. In PUF2**, the interface between the β 2- α 2 loop and the C-terminal end of α 3 is disordered, as are the α 1- β 2 loop and β 2. Mutations of the evolutionarily conserved aromatic residues reduce the energy gap between the N state and PUF2** as well as the previously identified PUF1, making both PUF1 and PUF2** more accessible from the N state in the mutant variants. This study also reveals that there are multiple misfolding pathways for moPrP. The observed misfolding rate constant of the mutant variants correlates well with the extents to which both PUF1 and PUF2** are populated at equilibrium, indicating that both PUF1 and PUF2** can directly misfold. On the other hand, a previous study had identified another aggregation-prone partially identified conformation, PUF2* (Pal & Udgaonkar, 2022), which is very similar in energy to PUF2** but has a very different conformation.

2 | MATERIALS AND METHODS

2.1 | Buffers and reagents

The reagents used in this study were of high purity grade and were obtained from Sigma. Ultra-pure guanidine hydrochloride (GdnHCl) of the highest purity grade was procured from United States Biochemicals [Alfa Aiser, catalog number-J75823].

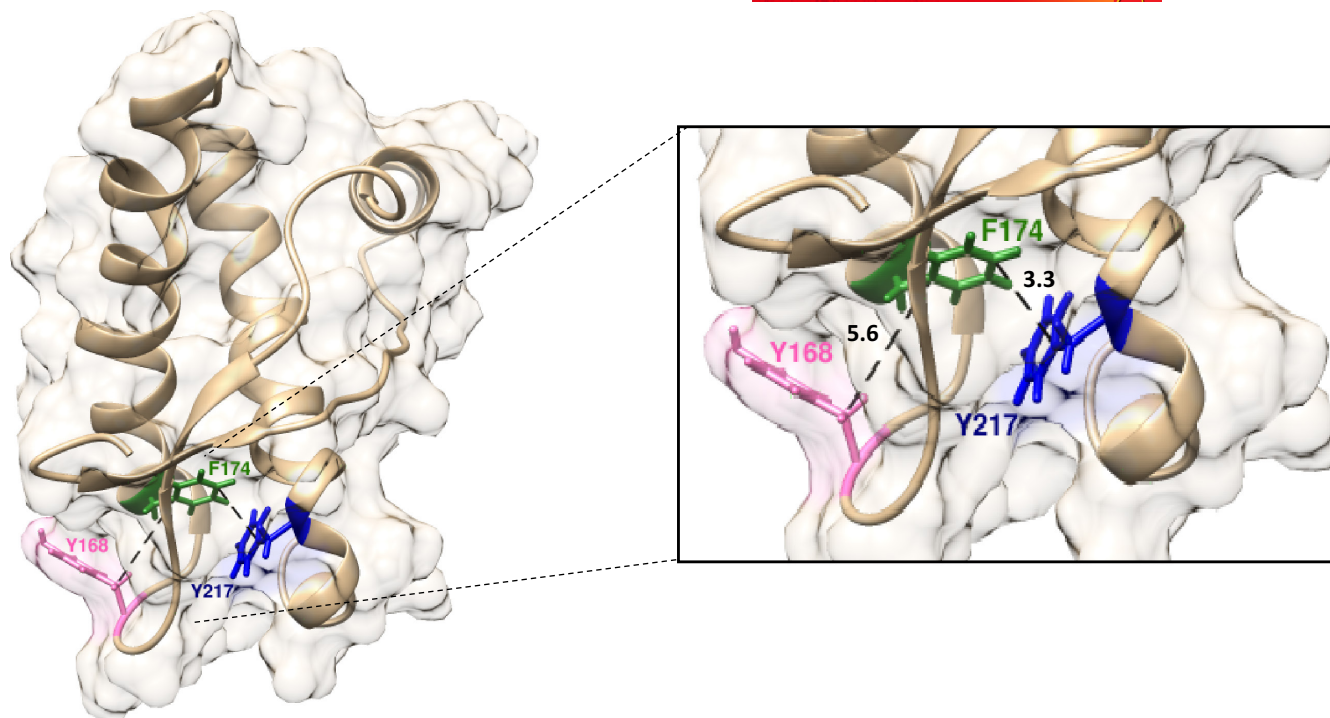


FIGURE 1 Structure of the C-terminal domain of the mouse prion protein showing the locations of the three conserved aromatic residues, Tyr168, Phe174, and Tyr217. The N-terminal domain comprises residues 23–120, and is unstructured in the full-length protein. The three conserved aromatic residues are colored pink (Y168), green (F174) and blue (Y217). The side-chains of Y168, F174, and Y217 are buried to the extents of 40%, 100%, and 90%, respectively. The distances between the side-chains are shown in Å in the expanded view. The figure was drawn using Chimera and Protein Data Bank entry 1AG2.

2.2 | Site-directed mutagenesis

Mutant variants of full-length moPrP were generated using the Quickchange site-directed mutagenesis kit (Stratagene, catalog number-200518). Primers containing 3 nucleotide changes were obtained from Sigma. Three mutant variants were prepared: Y168A, F174A, and Y217A moPrP. The mutations were confirmed by DNA sequencing.

2.3 | Protein expression and purification

wt moPrP and the mutant variants were expressed in *Escherichia coli* BL21(DE3) codon plus cells (Stratagene) transformed with a pET17b plasmid [RRID: Addgene_173032] containing the full-length sequence (23–231) of the moPrP gene. The moPrP variants were purified, as described previously (Jain & Udgaonkar, 2008; Singh et al., 2014). The purity and mass of each moPrP variant preparation were confirmed by mass spectrometry using a Synapt G2 HD mass spectrometer (Waters Corporation).

2.4 | Far-UV CD measurements

Far-UV CD spectra were recorded on a Jasco J-815 spectropolarimeter using a protein concentration of 10 μM in a 1 mm cuvette,

using a scan speed of 50 nm/min, a digital integration time of 2 s, and a bandwidth of 1 nm. The wavelength was scanned from 200 to 250 nm, and a total of 15 spectra were averaged. Far-UV CD spectra under native conditions were acquired in 10 mM sodium acetate [Sigma-Aldrich, catalog number-S2889], pH 4, at 25°C.

2.5 | Urea-induced equilibrium unfolding studies

Urea-induced equilibrium unfolding studies were carried out in 10 mM sodium acetate buffer at pH 4, at 25°C. 10 μM protein was incubated in different urea concentrations for 1 h, before the far-UV CD signal at 222 nm was monitored. The data were fit to a two-state N ↔ U equilibrium unfolding model (Agashe & Udgaonkar, 1995), and the thermodynamic parameters were obtained. Ultra-pure urea of the highest purity grade was procured from Sigma-Aldrich, catalog number-51458.

2.6 | Misfolding studies at pH 4

Misfolding was initiated by diluting 20 μM protein in 10 mM sodium acetate buffer (pH 4) two-fold with 2× misfolding buffer (10 mM sodium acetate buffer containing 300 mM NaCl [Sigma-Aldrich, catalog number-746398], pH 4). Both the protein sample and 2× misfolding buffer were incubated at 37°C before starting

the reaction. The time from the mixing of the protein solution with 2x misfolding buffer to the first reading was 20s. To study the misfolding kinetics of the moPrP variants, the CD signal at 222 nm (0222) was monitored using a 1 mm quartz cuvette maintained at 37°C.

2.7 | HDX-MS measurements

The peptide map of the moPrP variants was generated, as described previously (Pal & Udgaonkar, 2022). To initiate deuterium labeling, 100 μM protein was diluted into a labeling buffer [10 mM sodium acetate buffer in D₂O [Sigma-Aldrich, catalog number-151882] at pH 4, corrected for the isotope effect], so that HDX occurred in 95% D₂O, at 25°C. At different times, a 50 μL aliquot was mixed with 50 μL ice-cold 20 mM glycine-HCl buffer [Sigma-Aldrich, catalog number-50046] (pH 2.5) to quench the labeling reaction. Online pepsin digestion was carried out by injecting the samples immediately into an immobilized pepsin cartridge [Applied Biosystems, catalog number-39634] at a flow rate of 40 μL/min of water (0.05% formic acid, Sigma Aldrich, catalog number-106 526) which was placed in an HDX module (Waters Corporation) coupled to a nanoAcquity UPLC. The peptides eluting from the pepsin column were collected using a trap column [Waters, catalog number-186003975], washed to remove salt, and eluted over 12 min on an analytical C18 reversed-phase chromatography column [Waters, catalog number-18602346] using a gradient of 3–40% acetonitrile [Sigma Aldrich, catalog number-100 029], (0.1% formic acid) at a flow rate of 40 μL/min. All columns were kept at 4°C to minimize back exchange. The parameters of the mass spectrometer were set as follows: source temperature, 35°C; desolvation temperature, 100°C; capillary voltage, 3.0 kV.

Peptide masses were calculated from the centroid of the isotopic envelope, using MassLynx. The shifts in the masses of labeled peptides relative to unlabeled peptides were used to determine the extent of deuterium incorporation at each time point of HDX. Since the sample was in 95% D₂O during labeling, and exposed to H₂O during quenching, control experiments were carried out to correct for back exchange. For this, the protein was incubated in 10 mM sodium acetate, pH 4 (in 95% D₂O), and deuterated by unfolding at 65°C for 15 min, followed by refolding on ice. CD spectroscopy and thermal equilibrium unfolding studies showed that the refolded protein behaves like native moPrP. The fully (95%) deuterated moPrP samples were processed in the same way as the labeling reaction samples. The extent of deuterium incorporation in each peptide fragment, % D, was calculated using the equation:

$$\% D = \frac{(m(t) - m(0\%))}{(m(95\%) - m(0\%))} \times 100$$

where $m(t)$ is the measured centroid mass at time t , $m(0\%)$ is the measured mass of the undeuterated reference peptide, and $m(95\%)$ is the measured mass of the 95% deuterated reference peptide.

In the current study, native state HDX was performed in the EX2 limit (Moulick et al., 2019; Pal & Udgaonkar, 2022) allowing the stabilities of the partially unfolded forms, into which HDX occurs, to be determined. For calculation of the free energy of opening (ΔG_{op}) of a sequence segment, the observed HDX rate constant (k_{obs}) of deuterium incorporation was first obtained by fitting the kinetic curve of HDX to either a single exponential or a two-exponential equation, depending upon the goodness of fit. When the kinetic curve was fit to a two-exponential equation, k_{obs} was determined as the amplitude-weighted average of the two rate constants. In cases where the kinetic curves had yet to reach 100% deuterium incorporation at 1000 min, the fit was constrained to reach 100% at $t = \text{infinity} (\infty)$, except in the case of sequence segment 205–212 of wt protein.

For each of the sequence segments, k_{obs} was compared to the rate constant (k_{int}) that would be observed in the corresponding peptide fragment in a random coil state (Bai et al., 1993; Nguyen et al., 2018). The quantity $P_f = k_{int}/k_{obs}$ is the protection factor that slows down HDX into the sequence segment. The HDX protection factor determined for each peptide fragment was used to calculate the local stability of the corresponding sequence segment in the protein, $\Delta G_{op} = RT \ln P_f$. For each sequence segment, ΔG_{op} is therefore the free energy of opening of the N state to form an HDX-competent partially unfolded form.

2.8 | Statistical analysis of the free energy levels of the PUFs of the different moPrP variants

One-way ANOVA comparison tests, commonly used to assess significant distinctions between the means of multiple groups, were used to evaluate the significance of the differences in the free energy levels of the PUFs of the different moPrP variants. Data are represented as mean \pm SD of three independent experiments, with all statistical analysis performed using the GraphPad Prism software (version 10.0.3). Details of the statistical analysis are shown in Table S4.

3 | RESULTS

3.1 | Mutation of the aromatic residues affects stability but not secondary structure

All three single mutant variants showed far-UV CD spectra that are very similar to that of wt moPrP (Figure 2a), indicating that the Y168A, F174A, and Y217A mutations did not affect the global secondary structure of the protein. However, urea-induced equilibrium studies indicated that these mutations led to significant destabilization of the N state of the protein (Figure 2b; Figure S1). Y217A moPrP showed the highest degree of destabilization among the mutant variants ($\Delta\Delta G_{NU} = 2.4 \text{ kcal mol}^{-1}$), followed by F174A ($\Delta\Delta G_{NU} = 2.2 \text{ kcal mol}^{-1}$) and Y168A ($\Delta\Delta G_{NU} = 1.9 \text{ kcal mol}^{-1}$) moPrP,

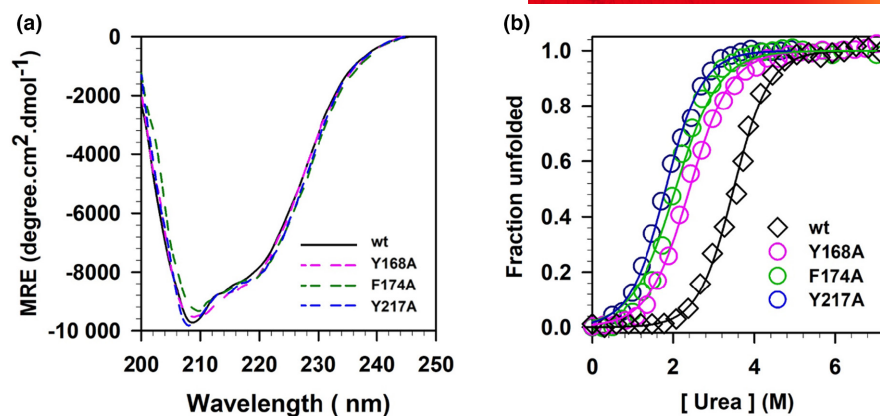


FIGURE 2 Effect of the mutations on secondary structure and stability (a) Far-UV CD spectra of the native monomeric forms of the moPrP variants acquired at pH4, 25°C. (b) Urea-induced equilibrium unfolding transitions of the moPrP variants at pH4, 25°C, as monitored by measurement of the far-UV CD signal at 222 nm. Spectra and unfolding transitions were obtained from three independent experiments, and representative spectra and unfolding transitions are shown. The signal change was normalized to obtain the fraction unfolded. The colors of the lines represent the different moPrP variants as indicated. The solid lines through the data points are fits to an equation describing a two-state unfolding transition.

suggesting that the conserved aromatic residues are important in maintaining the stability of the native protein.

3.2 | Mutation of the aromatic residues results in rapid misfolding

The prion protein is known to misfold on the cell surface, as well as in the endocytic pathway when it enters lysosomes and encounters a low pH (Borchelt et al., 1992). At pH4, moPrP remains in its native monomeric helix-rich conformation, but becomes prone to misfolding due to protonation of the critical residue His186 (Singh & Udgaonkar, 2016a). The misfolding of wt moPrP at pH4 in the absence of added salt, which would disrupt electrostatic interactions, is very slow ($\sim 10^{-4} \text{ h}^{-1}$) (Sengupta et al., 2017). Hence, in the current study, the misfolding of the different moPrP variants at pH4 was studied in the presence of a physiological concentration (150 mM) of NaCl at 37°C. The kinetics of misfolding were monitored by measuring the change in the CD signal at 222 nm. For all the moPrP variants, the kinetics of misfolding appeared monophasic and fit well to a single exponential equation. It should be noted that the misfolding of moPrP at pH4 is accompanied by oligomerization (Sabareesan & Udgaonkar, 2016; Sengupta & Udgaonkar, 2019). Earlier studies had shown that the kinetics of CD-monitored misfolding and the kinetics of oligomerization monitored by size exclusion chromatography (SEC) were identical for wt moPrP, suggesting that both processes occur concurrently (Sabareesan & Udgaonkar, 2016). All three mutant variants studied here misfold very much faster than wt moPrP (Figure 3a, b; Figure S1, S1 and Table S1), suggesting that the three conserved aromatic residues might have been evolutionarily selected to impede misfolding. Among the mutant variants, Y217A moPrP misfolded the fastest, followed by F174A and Y168A moPrP.

3.3 | Dependence of the rate constants of misfolding on native state stability

Table S1 shows the effects of the mutations on the stability of the N state and the observed rate constant of misfolding. In Figure 3c, the observed rate constants of misfolding are plotted against the decrease in free energy of unfolding ($\Delta\Delta G_{\text{NU}}$) of the mutant variants with respect to wt moPrP (Figure 3c). The logarithm of the observed misfolding rate constant increased linearly with the extent of destabilization ($\Delta\Delta G_{\text{NU}}$). Several disease-linked mutant variants are known to misfold rapidly under similar conditions, and for them too, a linear dependence of the logarithm of the observed misfolding rate constants on the decrease in the free energy of unfolding ($\Delta\Delta G_{\text{NU}}$) has been observed (Singh & Udgaonkar, 2015, 2016b). Interestingly, the observed misfolding rate constants of the mutant variants studied here, and of the disease-linked mutant variants studied earlier, have the same dependence on $\Delta\Delta G_{\text{NU}}$ (Figure 3c).

3.4 | Effect of mutation of the aromatic residues on protein dynamics

To determine the effect of the mutations not only on the structure but also on the dynamics of the protein, HDX-MS studies were carried out. The HDX-MS studies revealed sequence-specific information about changes in the structure and dynamics that occurred upon mutation. The HDX experiments were carried out at pH4, where the intrinsic rate constant of HDX is slow (Bai et al., 1993). This allowed HDX to be monitored at amide hydrogen sites spread over all the secondary structural elements of the protein.

Figure 4 shows the kinetics of deuterium incorporation into different sequence segments of the CTD of moPrP, for the different mutant variants. The sequence segments covering $\alpha 1$ (144–148,

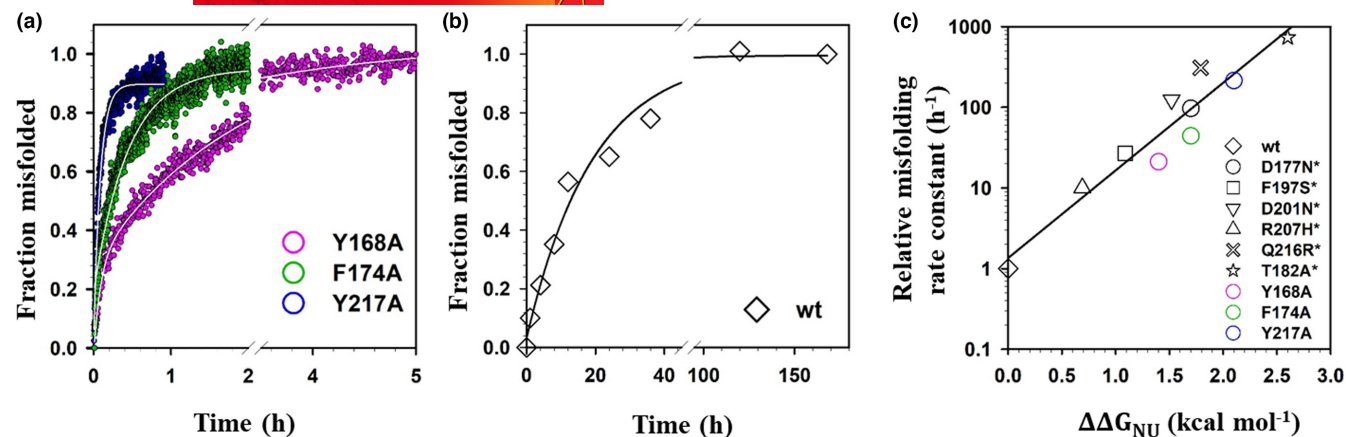


FIGURE 3 Dependence of the observed rate constant of misfolding on native state stability (a) The fraction misfolded form at different times of misfolding in 150 mM NaCl at pH4, 37°C of 10 μM Y168A, F174A, and Y217A moPrP (a) and of 10 μM wt moPrP (b) are shown. The fraction misfolded form was calculated from the fractional change in the CD signal at 222 nm. The continuous lines through the data points in both panels a and b are fits to an exponential equation. (c) Plot of the relative observed rate constant of misfolding of the different moPrP variants in 150 mM NaCl at pH4, at 37°C versus the decrease in global stability of the mutant variants ($\Delta\Delta G_{\text{NU}}$) with respect to wt moPrP. The misfolding of the single aromatic mutant variants was studied at 10 μM concentration, and that of the disease-linked mutant variants was studied at 100 μM concentration. Kinetic misfolding curves were obtained from three independent experiments, and representative data are shown. The continuous line through the data points are linear fits to the data points. For both sets of mutant variants, the misfolding rate constants were normalized to a value of 1 for the misfolding rate constant of 10 and 100 μM wt moPrP. Asterisks denote data for disease-linked mutant variants, which was taken from references Singh & Udgaonkar, 2015, 2016b.

149–153), part of $\alpha 2$ (177–183) and the loop between $\alpha 2$ and $\alpha 3$ and the N terminal ends of $\alpha 3$ (197–204) showed little or no variation in the kinetics of deuterium incorporation in the mutant variants compared to that in wt moPrP (except sequence segment 177–183 in the case of Y168A moPrP). The kinetics of deuterium incorporation were found to be faster in most of the other sequence segments for the mutant variants. For sequence segments 96–144 spanning $\beta 1$, 168–173 spanning the loop between $\beta 2$ and $\alpha 2$, 182–196 spanning the C-terminal end of $\alpha 2$ (182–196), 210–216 spanning the second half of $\alpha 3$, and 225–231 at the C-terminus of the protein, the observed rate constants were only 2–10 faster for the mutant proteins than for the wt protein (Figure S2; Table S2). It should, however, be noted that in the case of the wt protein, the k_{obs} values for these sequence segments were less than 10-fold faster than the corresponding k_{int} values. For sequence segment 154–167 spanning the loop between $\alpha 1$ and $\beta 2$, and $\beta 2$ the observed rate constants of deuterium incorporation (k_{obs}) were significantly faster for all three mutant variants than for wt moPrP (Table S2). Sequence segment 205–212 spanning the first half of $\alpha 3$ as well as sequence segment 217–223 spanning the C-terminal end of $\alpha 3$, showed significant increases in k_{obs} values for two of the three mutant variants.

Figure 5 and Figure S3 show the ΔG_{op} values of the different sequence segments of the mutant variants studied here. It shows that the mutations principally decreased the ΔG_{op} values for the sequence segments of $\alpha 3$ (205–212, 210–216, and 217–223), along with the sequence segments of $\beta 1$ (96–144), the loop between $\alpha 1$ and $\beta 2$, and the $\beta 2$ (154–167), the loop between $\beta 2$ and $\alpha 2$ (168–173), the C-terminal end of $\alpha 2$ (182–196) and the C-terminal end of the protein (225–231). Since the conserved aromatic residues form a very stable network of aromatic interactions spanning the loop

between $\alpha 1$ and $\beta 2$, $\beta 2$ (154–167) and the loop between $\beta 2$ and $\alpha 2$ (168–173) and the C-terminal end of $\alpha 3$ (210–216, 217–223) and 225–231 (Figure 1) their mutation decreased the local stabilities (ΔG_{op}) of these sequence segments (Figure 5; Table S3). This suggests that the mutations principally affected the local stabilities of the sequence segments near the sites of the mutations. It is interesting that sequence segments 96–144 and 182–196 also showed reduced ΔG_{op} values upon mutation, even though they are far from the sites of the mutations.

3.5 | Identification of partially unfolded forms in equilibrium with the N state

Previous HDX-NMR and HDX-MS measurements had identified two sparsely populated, partially unfolded forms (PUFs), PUF1 and PUF2, in dynamic equilibrium with the N state, in the case of both isolated CTD (Moulick et al., 2015; Moulick & Udgaonkar, 2017) and full-length wt moPrP (Pal & Udgaonkar, 2022). PUF2 was more disordered than PUF1; it had more regions that had lost intramolecular hydrogen bonding and become fully solvent-exposed, and hence unprotected against HDX. In the case of wt moPrP, PUF1 was characterized by a local stability (ΔG_{op}) of $1.3 \pm 0.2 \text{ kcal mol}^{-1}$, whereas PUF2 was characterized by a higher local stability (ΔG_{op}) of $3.3 \pm 0.2 \text{ kcal mol}^{-1}$ (Moulick et al., 2015; Pal & Udgaonkar, 2022). The current study not only confirmed the existence of PUF1 and PUF2 in the case of wt moPrP but also determined the effects of the mutations of the conserved aromatic residues on the stabilities of the two PUFs. These mutations were found to increase the sampling of both PUFs from the N state by

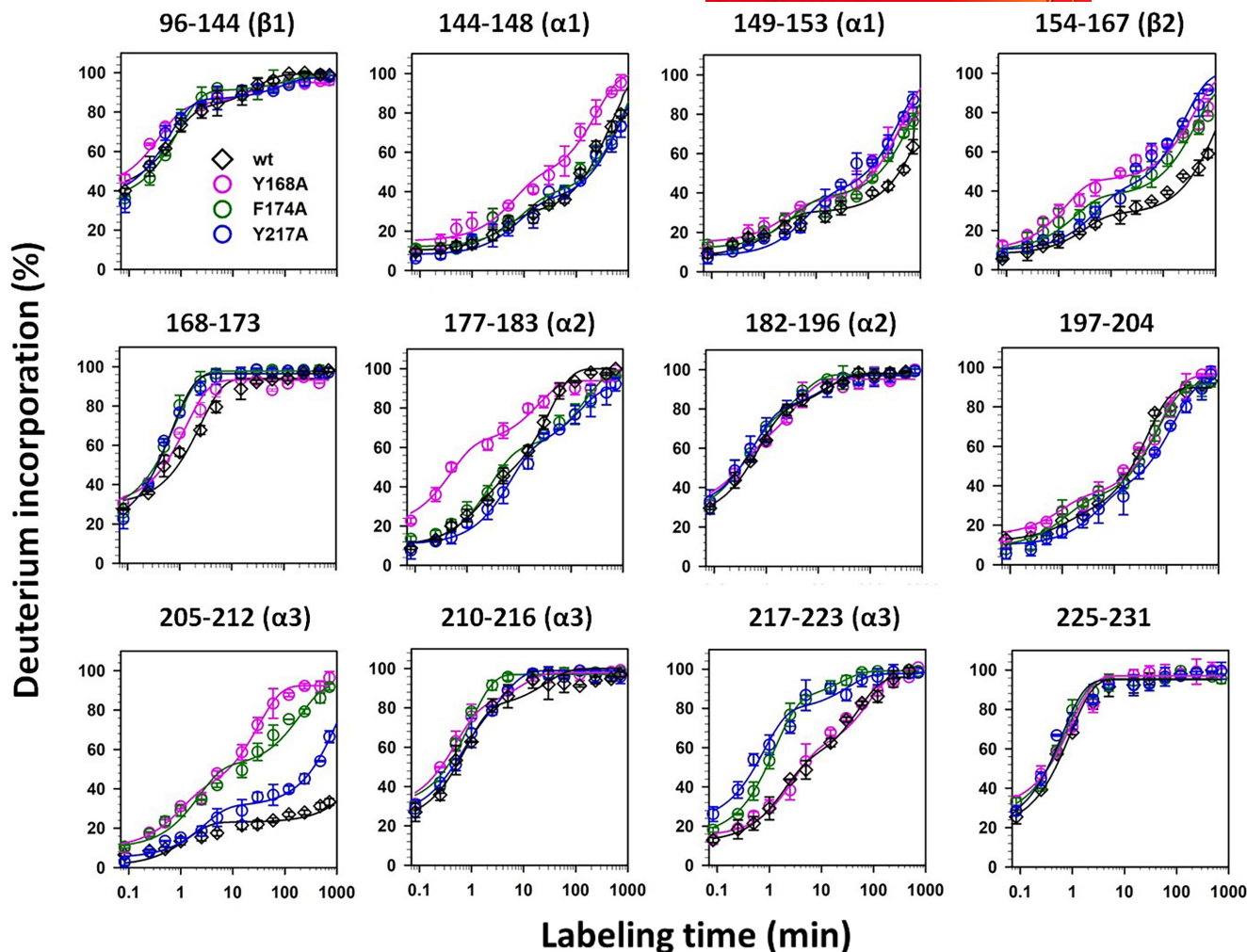


FIGURE 4 Effect of the mutations on the native state dynamics. The time courses of HDX into different sequence segments of the native states of the moPrP variants at pH4, 25°C are shown. The black diamonds represent wt moPrP, and the differently colored circles represent the mutant moPrP variants, as indicated. Each data point represents the mean value obtained from three independent experiments, and the error bars represent the standard deviations of measurement. For some data points, the error bars fall within the size of the symbol. The solid lines through the data represent fits to either monoexponential or biexponential equations.

decreasing the ΔG_{op} values of the sequence segments that exchange out in PUF1 and PUF2.

3.6 | Identification of PUF2**, a structurally distinct sub-population of PUF2

When PUF1 and PUF 2 were first identified by HDX-NMR and HDX-MS studies of moPrP as two distinct states that differed in structure and energy, it was assumed that each PUF consisted of a structurally homogenous population of molecules (Moulick et al., 2015), and not of iso-energetic sub-populations differing in their structures. The first evidence for conformational heterogeneity in PUF2 came from the HDX-MS characterization of *Pro* to *Ala* mutant variants of moPrP (Pal & Udgaonkar, 2022), which identified a sub-population of PUF2, called PUF2**, which was disordered in only some of the sequence segments known to have become disordered

in PUF2, but which had a local stability (ΔG_{op}) of 3.7 ± 0.4 kcal mol⁻¹ (Pal & Udgaonkar, 2022). Of the sequence segments known to be disordered in PUF2, PUF2** had sequence segments 144–148, 149–153, 154–167, and 197–204 disordered (Figure 6), but not sequence segments 177–183 and 217–223. That study suggested that in addition to the sub-population PUF2**, PUF2 must consist of another isoenergetic sub-population in which sequence segments 177–183 and 217–223, and possibly other sequence segments, had become disordered.

Of the sequence segments known to be disordered in PUF2, only sequence segments 154–167 (the loop between $\alpha 1$ and $\beta 2$, and the $\beta 2$) and 217–223 (the C-terminal end of $\alpha 3$) became disordered upon mutation of the conserved aromatic residues (Figure 5). Importantly, the sequence segments known to be disordered in PUF2* (Pal & Udgaonkar, 2022) were not affected, except for sequence segment 154–167. Hence, the effects of the mutations of the three aromatic residues suggested that there exists a second

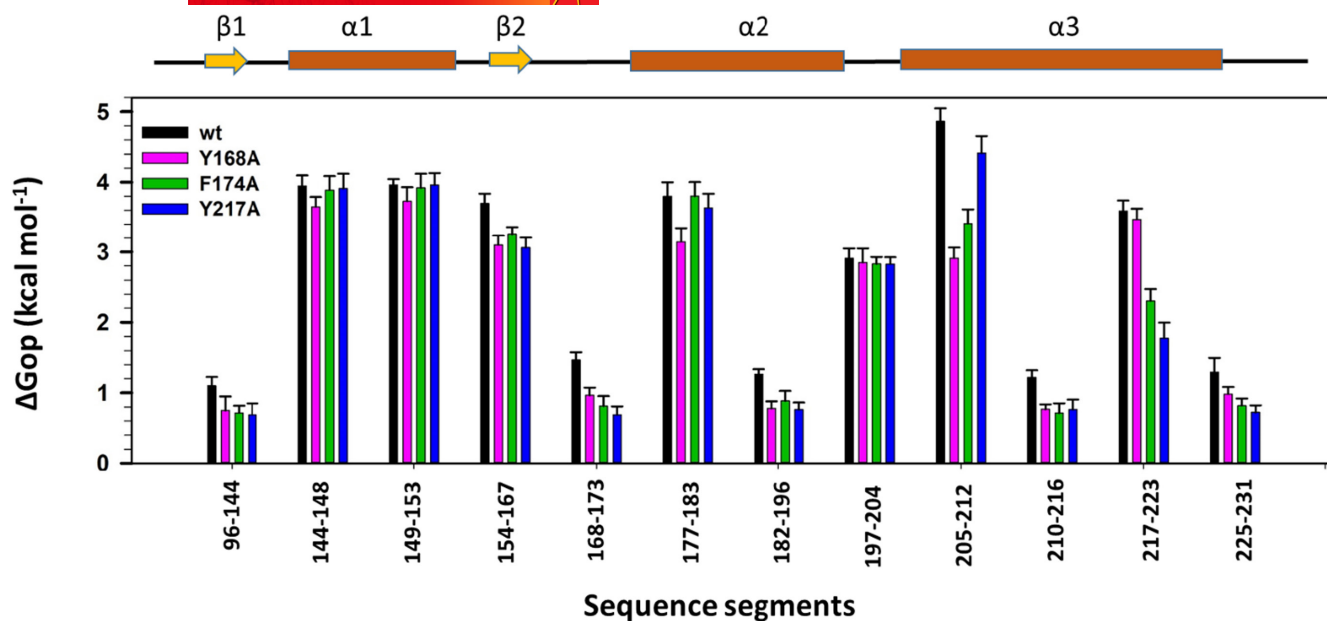


FIGURE 5 ΔG_{op} values of the different sequence segments of the aromatic mutant variants. The secondary structural elements coded for by the sequence are shown above the sequence segments (rectangular boxes represent the α -helices, and arrows represent the β -strands). The differently colored bars represent the different moPrP variants, as indicated. The error bars represent the standard deviations determined from three independent experiments.

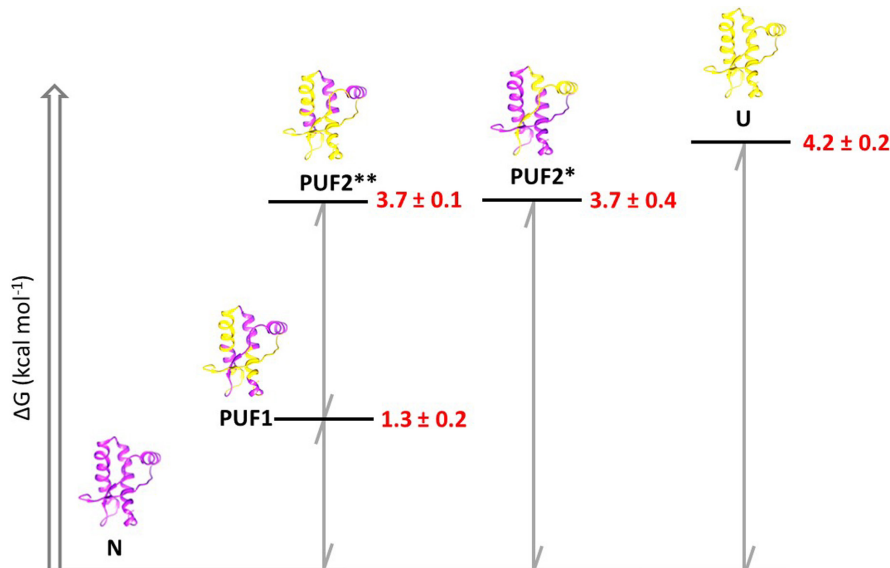


FIGURE 6 Stabilities (ΔG) of the native and partially unfolded forms of wt moPrP at pH4 as identified by native state HDX-MS. PUF1 appears to be a homogenous population of molecules. PUF2 is shown to comprise two isoenergetic sub-populations of molecules, PUF2* and PUF2**, which differ in structure. For each PUF, segments that are intact in structure are shown in purple, while those that have unfolded are shown in gold. The stabilities of the individual PUFs are shown in red. It appears that the perturbation of different elements of structure, $\alpha 1$ and the spatially adjacent N-terminal end of $\alpha 2$ in PUF2*, and the $\beta 2$ - $\alpha 2$ loop and the C-terminal end of $\alpha 3$ in PUF2**, can lead to the same extent of destabilization. The different forms (PUF1, PUF2*, PUF2** and U) in dynamic equilibrium with the N state will be populated in accordance with Boltzmann's Law. Hence, while it has been shown (see text) that misfolding can potentially commence from any of the three PUFs shown, it will occur predominantly from PUF1 which only is populated to a significant extent.

sub-population of PUF2, designated here as PUF2**, in which sequence segments 154–167 and 217–223 have become disordered (Figure 6). In the case of wt moPrP, the local stability (ΔG_{op}^{av}) of PUF2**, determined by averaging the ΔG_{op} values of sequence segments 154–167 and 217–223, is 3.7 ± 0.1 kcal mol⁻¹. Mutation

of the aromatic residues also has a significant impact on sequence segments 96–144, 168–173, 182–196, 210–216, and 225–231, which were known to be disordered in PUF1, and it is likely that these segments are also disordered in PUF2**, as indicated in Figure 6 and discussed later.

3.7 | Effect of mutation of the aromatic residues on the stabilities of the PUFs

The mutations of the conserved aromatic residues had a significant impact on the stability with respect to the unfolded (U) state of each PUF ($\Delta G_{PU} = \Delta G_{NU} - \Delta G_{op}$) for each protein variant. In the case of PUF1, the ΔG_{PU} value was found to be equal to about 0.7 ΔG_{NU} for wt moPrP, indicating that PUF1 retains approximately 70% of the stabilizing interactions that were originally present in the native state of wt moPrP (Table S3; Figure S4). Although the ΔG_{PU} values for the three mutant variants are different from each other, they all fall in the range of 0.61–0.69 times the ΔG_{NU} value (Figure S4). Consequently, it can be concluded that, on averaging the ΔG_{PU} values for PUF1 of the three mutant variants, the stability of PUF1 in each of the mutant variants is about half the stability in the case of wt moPrP. Hence, it appears that PUF1 of the mutant variants is stabilized by only about 45% of the stabilizing interactions that are present in the N state of wt moPrP.

In the case of PUF2**, the ΔG_{PU} value was found to be approximately 0.25 ΔG_{NU} for wt moPrP (Figure S4). This result suggested that, in the case of wt moPrP, PUF2** possesses only 25% of the stabilizing interactions that are present in the N state. However, for the mutant variants, the ΔG_{op} values for PUF2** were higher than their corresponding ΔG_{NU} values (Figure S4), suggesting that PUF2** was a high energy intermediate form less stable than the U state. The data cannot distinguish between PUF2** being on or off the pathway from the N state to the U state. It would appear that the U state of the mutant variants is stabilized by residual structure that is absent in the U state of wt mPrP, as suggested for other proteins (Park & Marqusee, 2004; Wedemeyer et al., 2002; Wrabl & Shortle, 1999). Such stabilizing residual structure would be absent in PUF2**.

3.8 | Effect of the mutations on the sequence segment not disordered in PUF2

In the case of wt moPrP, sequence segment 205–212 did not become disordered (open to HDX) in either PUF1 or PUF 2, and its ΔG_{op} value suggested that it becomes disordered only in the U state (Moulick et al., 2015). While this sequence segment appeared to be impacted by all three mutations (Figure 5), the impact was found to be significant in the case of Y168A and F174A moPrP. For these two mutant variants, the ΔG_{op} value was lowered to a value equal to the ΔG_{op} value for PUF2 (Figure 5), suggesting that this segment may have lost structure in PUF2 itself. It could not, however, be determined whether this segment has lost structure in PUF2**.

3.9 | Misfolding rate constants of the mutant variants correlate with their local stabilities

The logarithm of the observed rate constant of misfolding of the mutant variants was found to increase linearly with the decrease in the

average of the ΔG_{op} values (ΔG_{op}^{av}), for the sequence segments that exchange out in PUF1 (96–144, 168–173, 182–196, 210–216, and 225–231; Figure S6) as well as those that exchange out in PUF2** (154–167 and 217–223) (Figure S7). As the logarithm of the observed misfolding rate constant correlates well with the equilibrium populations of PUF1 as well as of PUF2**, it appears that both PUFs can act as precursors to misfolding.

The dependences of the logarithm of misfolding rate constant on ΔG_{op} for PUF1 and for PUF2** were a bit different (Figure 7a). Interestingly, when the logarithm of the observed rate constant of misfolding of the mutant variants was plotted against the fractional destabilization (calculated as $[(\Delta G_{op}^{wt} - \Delta G_{op}^{mutant})/\Delta G_{op}^{wt}]$), of the sequence segments that are unstructured in PUF1 (sequence segments 96–144, 168–173, 182–196, 210–216, 225–231) as well as in PUF2** (sequence segments 154–167 and 217–223), the linear dependences were found to be same for both PUFs (Figure 7b).

4 | DISCUSSION

4.1 | Mutation of the conserved aromatic amino acids destabilize the N state

The observation that the mutations of the conserved aromatic residue to Ala reduces the free energy of unfolding (ΔG_{NU}) can be rationalized to be the result of enthalpic destabilization of the N state. The network of stabilizing interactions by the three aromatic residues would be perturbed in the mutant variants. The side-chains of Phe174 and Tyr217 are 100% and 90% buried, respectively, and are also part of the hydrophobic core of the protein, in addition to being part of the network of aromatic contacts. Mutation of Phe174 or Tyr217 to the smaller Ala is expected to create a cavity and to perturb the packing of the core. The occurrence of cavities within the hydrophobic core of a protein is known to have a strong destabilizing effect on the N state (Jackson et al., 1993). Not surprisingly, mutation of Tyr168, whose side chain is only 40% buried, has a weaker destabilizing effect than do the mutations of Phe174 and Tyr217. However, it appears from NMR and MD simulation studies that the Tyr168 hydroxyl group and the Asp177 carboxyl group form a very stable H-bond (Caldarulo et al., 2017; Huang & Caflisch, 2015). The reduced stability of the Y168A mutant variant can be rationalized by invoking the loss of this stabilizing interaction, as well as the loss of stabilizing stacking interactions with Phe174. The combined effect of disruption of these stabilizing interactions has a synergistic impact, causing the mutant variants studied here to have a markedly destabilized N state.

4.2 | Heterogeneity in PUF2

The current study has identified a sub-population, PUF2**, in the PUF2 ensemble that is structurally distinct from a previously

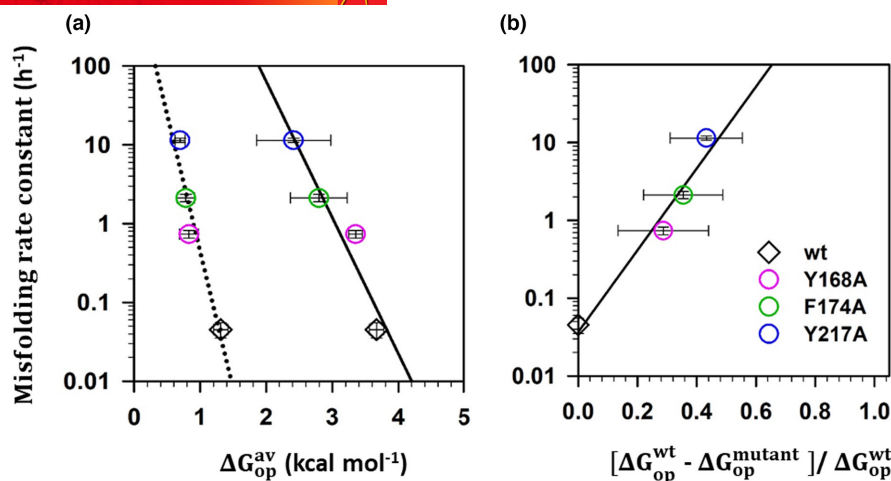


FIGURE 7 Dependence of the observed misfolding rate constant on ΔG_{op} for different sequence segments. (a) Plot of the dependence of the observed rate constant of misfolding of the aromatic mutant variants at 10 μ M concentration in 150 mM NaCl at pH4, 37°C on the stability (ΔG_{op}^{av}) of PUF1 (dotted line) and PUF2** (solid line). The stabilities (ΔG_{op}^{av}) of PUF1 and PUF2** were determined by averaging the ΔG_{op} values of the sequence segments 96–144, 168–173, 182–196, 210–216, and 225–231 for PUF1 and 154–167 and 217–223 for PUF2**. The continuous lines through the data points are linear fits. (b) Plot of the dependence of the observed rate constant of misfolding of the single aromatic mutant variants at 10 μ M concentration in 150 mM NaCl at pH4, at 37°C on the fractional destabilization of the sequence segments 96–144, 154–167, 168–173, 182–196, 210–216, 217–223, and 225–231. Each data point represents the fractional destabilization averaged over these seven sequence segments. The continuous lines through the data points are linear fits. The error bars represent the standard deviations determined from three independent experiments.

identified sub-population, PUF2* (Pal & Udgaonkar, 2022). PUF2* is disordered in $\alpha 1$ (sequence segments 144–148, 149–153), the loop between $\alpha 1$ and $\beta 2$ and $\beta 2$ (sequence segment 154–167), and the loop between $\alpha 2$ and $\alpha 3$ as well as the N-terminal end of $\alpha 3$ (sequence segment 197–204; Figure 6). In contrast, PUF2** is not disordered in these regions except for the loop between $\alpha 1$ and $\beta 2$ and $\beta 2$ (sequence segment 154–167), and is disordered also at the C-terminal end of $\alpha 3$ (sequence segment 217–223; Figure 6). Neither PUF2* nor PUF2** are disordered in sequence segment 177–183, which is known to be disordered in PUF2, suggesting that PUF2 must comprise other sub-populations of distinct conformations.

Hence, the N state of moPrP is in dynamic equilibrium with at least two PUF2s, which have distinct conformations, but which nevertheless have similar stabilities. This result is supportive of energy landscape theories of protein folding which posit that completely different conformations may have similar energies (Eaton & Wolynes, 2017).

4.3 | PUF1 and PUF2** may form either sequentially or in parallel from the N state

It has been suggested that protein unfolding occurs by the sequential loss of blocks of secondary structure (Hughson et al., 1990), and for several proteins, including apomyoglobin (Hughson et al., 1990), cytochrome c (Hu et al., 2016), and ribonuclease H (Hu et al., 2013), partially unfolded forms have been shown to be populated sparsely, in equilibrium with the N state. For cytochrome c and ribonuclease H, PUFs could be placed on a ladder of increasing disorder from the

N to U state, as determined from their ΔG_{op} values and their exposures to solvent. In this way, PUFs were assumed to form on a sequential unfolding pathway from the N to U state, with regions unfolded in a PUF of lower ΔG_{op} value being also unfolded in a PUF of higher ΔG_{op} value. A PUF was assumed to be a homogeneous population of molecules, and not instead be a heterogeneous mix of sub-populations with different structures. In the case of moPrP, since the ΔG_{op} value of PUF2 was found to be higher than that of PUF1 (Moulick et al., 2015; Pal & Udgaonkar, 2022), it appeared that PUF1 was on the pathway of unfolding of the N state to PUF2, and, consequently that the sequence segments that were unfolded in PUF1 were also unfolded in PUF2.

In the case of the aromatic mutations studied here, each mutation significantly destabilizes the N state as well as the PUFs. With respect to their stabilities in wt moPrP, the N state is destabilized the most, then PUF1, and PUF2 is destabilized the least, which is not surprising given that PUF2 would have less structure that can be destabilized. Unfortunately, while it appears that PUF1 and PUF2** are populated sequentially on the pathway of unfolding from the N to U state, it cannot be definitely concluded that this is the case. The observation that the dependence of the logarithm of the observed rate constant of misfolding on fractional localized destabilization (calculated by $G_{op}^{wt} -$) of PUF1 is the same as that of PUF2** (Figure 7b) suggests that PUF2** may populate from the N state via PUF1. If this is indeed so, then PUF2** would have $\beta 1$ (96–144), the $\alpha 1$ - $\beta 2$ loop, $\beta 2$ (154–167), the $\beta 2$ - $\alpha 2$ loop (168–173), the C-terminal end of $\alpha 2$ (182–196) and the second half (210–216) and C-terminal end of $\alpha 3$ (217–223) and sequence segment 225–231 all disordered at the main chain level. In Figure 6, it is evident that PUF1 is on the



pathway of unfolding from the N state to PUF2**, but it cannot, however, be ruled out at the present time that PUF1 and PUF2** form independently and in parallel from the N state.

4.4 | Misfolding can potentially commence from multiple PUFs

The observation that the logarithm of the observed rate constant of misfolding is linearly proportional to the free energy difference (ΔG_{op}) between the N state and PUF1 as well as PUF2** (Figure 7) suggests that misfolding can potentially commence from both these PUFs. An earlier study identified PUF2* as a precursor conformation from which misfolding begins in the case of full-length moPrP (Pal & Udgaonkar, 2022). Hence, it appears that misfolding can potentially commence from either of the two isoenergetic but structurally distinct sub-populations, PUF2* and PUF2**. Mutation of the conserved Pro residues (Zhang, 2015) affects the stability of PUF2*, while mutation of the conserved aromatic residues affects the stability of PUF2** (Figure S5). In this way, misfolding of different mutant variants may commence from or proceed via either PUF2* or PUF2**.

Misfolding will, however, predominantly begin from PUF1, as it is considerably more stable than both PUF2* and PUF2**, and would be populated >30-fold more than them at equilibrium. Hence, PUF1 would be the dominant precursor conformation from which misfolding commences. Misfolding can, however, begin, albeit to very small extents, from PUF2* and PUF2**, which have very different structures (Figure 6). If PUF1 is indeed populated on the pathways of unfolding from the N state to PUF2*, and from the N state to PUF2**, it is likely that it is the structure lost during the unfolding of the N state to PUF1, which makes all three PUFs competent to misfold. If PUF1 is not populated on the pathways of unfolding from the N state to PUF2*, and from the N state to PUF2**, then when misfolding commences from PUF1, additional structural loss and conformational conversion would occur only during the oligomerization process (Sengupta & Udgaonkar, 2019).

4.5 | Structure lost in PUF1 makes it prone to misfolding

It is important to determine what critical structure is lost in the PUFs which make them start to misfold. Misfolding rate constants will depend not only on the extent to which the PUFs are populated but also on the nature of the structural perturbation that has occurred to them. A mutation might lead to a small increase in the population of a PUF by changing its stability only to a small extent, but might yet have altered its structure in such a way that drastically lowers the barrier to misfolding.

In the case of PUF1, the sequence segments covering $\beta 1$ (96–144), the $\alpha 1$ - $\beta 2$ loop, the $\beta 2$ - $\alpha 2$ loop (168–173), the C-terminal end of $\alpha 2$ (182–196), the second half of $\alpha 3$ (210–216), and the sequence

segment 225–231 are found to have become disordered. An earlier NMR study of the temperature dependence of chemical shifts seen for wt moPrP (Bhate et al., 2021) had indicated that in the absence of added salt, many residues in $\beta 1$ and the $\beta 1$ - $\alpha 1$ loop (in sequence segment 96–144), as well as Gln211 in the second half of $\alpha 3$ (in sequence segment 210–216), which is adjacent in structure, sample at least one alternative conformation. Both these sequence segments are disordered in PUF1 suggesting that it is the alternative conformation that is sampled.

It is not yet known how the addition of the salt (150 mM NaCl) affects the extents to which the PUFs are populated. The NMR study of the temperature dependence of chemical shifts (Bhate et al., 2021), indicated that, upon the addition of the salt, the alternative conformation in which the residues in $\beta 1$ and the $\beta 1$ - $\alpha 1$ loop as well as Gln211 in the second half of $\alpha 3$ are perturbed (see above), becomes populated to a greater extent. This could mean that PUF1 becomes populated to a greater extent. Another NMR chemical shift study (Bai et al., 1993) also indicated that the salt bridge between Lys193 and Glu195 (in sequence segment 182–196 which is disordered in PUF1), as well as the local environment of Gln211, become structurally perturbed in the monomer upon the addition of the salt, before oligomerization commences. The very early perturbation of the salt bridge between Lys193 and Glu195 was also indicated in the burst phase change in the fluorescence of a Trp introduced at residue position 197, before misfolding commences (Nguyen et al., 2018). These previous results support the results of the current study that misfolding commences primarily from PUF1.

Of the sequence segments that have become disordered in PUF1, the C-terminal end of $\alpha 2$ (182–196) contains the sequence $^{187}\text{TVTTTT}^{192}$, which has a high propensity for β -sheet formation (Dima & Thirumalai, 2004), but is part of the helix $\alpha 2$. The $\beta 2$ - $\alpha 2$ loop (168–173) spans the sequence $^{169}\text{SNQNNF}^{174}$, and a peptide with this sequence is known to be highly amyloidogenic (Huang & Caflich, 2015). When these sequence segments become disordered in PUF1, they would become available for potential intermolecular interactions that facilitate misfolding. Moreover, the tertiary interactions between the $\beta 2$ - $\alpha 2$ loop and the second half of $\alpha 3$, which are known to play a crucial role in prion misfolding, are also perturbed in PUF1, making it prone to misfolding.

The $\beta 2$ - $\alpha 2$ loop interacts also with residues at the C-terminal end of $\alpha 3$, which are disordered in PUF2**, and perturbation of these intramolecular interactions would appear to be required for the formation of the specific intermolecular contacts that are involved in PrP conversion (Bett et al., 2012; Kurt, Bett, et al., 2014; Meli et al., 2011). It appears that mammals carrying a flexible $\beta 2$ - $\alpha 2$ loop are more easily infected than mammals with a rigid loop (Scialò et al., 2019; Zhang, 2011). In vivo as well as in vitro studies have revealed that several residues in the $\beta 2$ - $\alpha 2$ loop can regulate the formation of PrP^{Sc} by influencing the structural stability of this loop (Bett et al., 2012; Kurt, Bett, et al., 2014; Kurt, Jiang, et al., 2014; Sigurdson et al., 2011). PrP^C structures that are characterized by a rigid $\beta 2$ - $\alpha 2$ loop have a closer contact between the loop and the

C-terminal half of $\alpha 3$ (Scialò et al., 2019). The spontaneous formation of PrP^{Sc} in the cases of the E200K (Meli et al., 2011), Y217N (Jung Cheng & Daggett, 2014), V210I (Biljan et al., 2011), Q212P (Giachin et al., 2011), and Q226E (Slapšak et al., 2019) mutant variants, which are associated with familial prion diseases, is thought to be caused by the disruption of the long-range interactions between the $\beta 2$ - $\alpha 2$ loop and the C-terminal half of $\alpha 3$.

4.6 | Subdomain separation is facilitated by two different mechanisms

It has been proposed that during the misfolding of the prion protein, the separation of the $\alpha 2$ - $\alpha 3$ and the $\beta 1$ - $\alpha 1$ - $\beta 2$ subdomains must occur before the conversion of $\alpha 2$ and $\alpha 3$ to the β -conformation later during the misfolding process (Goluguri et al., 2019; Hadži et al., 2015; Sengupta & Udgaonkar, 2019). Locking of the $\alpha 2$ - $\alpha 3$ subdomain to the $\beta 1$ - $\alpha 1$ - $\beta 2$ subdomain by binding to anti-prion drugs (Kamatari et al., 2013; Kuwata et al., 2007), prevents misfolding and oligomerization, presumably by stabilizing the N state with respect to an aggregation-competent PUF. When a disulfide bond was introduced between the $\beta 2$ - $\alpha 2$ loop and the C-terminal half of $\alpha 3$, the formation of misfolded oligomers was significantly reduced, which suggested that the interactions between the two subdomains guarded against misfolding (Prigent & Rezaei, 2011). In the case of the mutant variants studied here, the perturbation of the aromatic and hydrophobic interactions between the $\beta 2$ - $\alpha 2$ loop and the C-terminal part of $\alpha 3$ appears to result in a decrease in the local stability of the $\beta 2$ - $\alpha 2$ loop. This loop serves as a hinge loop connecting the two subdomains, whose perturbation facilitates their separation. It seems that the decreases in the local stabilities (ΔG_{op}) of the sequence segments covering $\beta 1$ (96–144) and the C-terminal end of $\alpha 2$ (182–196), which are far from the site of mutations, is a consequence of the separation of the two subdomains.

Several disease-linked mutations (Singh & Udgaonkar, 2015), as well as mutations of the CTD Pro residues (Pal & Udgaonkar, 2022), facilitate subdomain separation by perturbing the electrostatic interaction network at one end of the protein. This electrostatic network is comprised of salt bridges formed by residues present on $\alpha 1$ of the $\beta 1$ - $\alpha 1$ - $\beta 2$ subdomain, and the loop between $\alpha 2$ and $\alpha 3$, and the N terminal end of $\alpha 3$ of the $\alpha 2$ - $\alpha 3$ subdomain (Figure S8a). In the case of the mutant variants studied here, this electrostatic interaction network is largely unaffected as the ΔG_{op} values of the sequence segments $\alpha 1$ (144–148, 149–153), and 197–204 (the loop between $\alpha 2$ and $\alpha 3$ and the N terminal end of $\alpha 3$) of the mutant variants were found to be same to those of wt moPrP. Nevertheless, subdomain separation appears to be facilitated by the perturbation of aromatic and hydrophobic interactions present at the other end of the protein (Figure S8b). This result reveals that subdomain separation can be triggered by two different structural mechanisms in which PUF1 can potentially misfold via both PUF2* and PUF2**, in which electrostatic interactions at one end and aromatic interactions at the other end of the protein, respectively, are perturbed.

A previous study utilizing force spectroscopy (Yu et al., 2012) had identified multiple, off-pathway partially structured intermediates that fold from the U state, but no structural information could be obtained, nor was it shown that they lead to misfolding. In a previous study utilizing fluorescence correlation spectroscopy, the N state was shown to be in rapid dynamic equilibrium with two native-like states (Goluguri et al., 2019), but, again, these states could not be characterized structurally. In this study, as well as in a previous study (Pal & Udgaonkar, 2022), the structures of partially unfolded forms (PUF1, PUF2* and PUF2**) from which misfolding can commence has been obtained. Both PUF2* and PUF2** have the same stability and would be populated equally at equilibrium. Since PUF2* and PUF2** differ in the regions of the protein structure that have become disordered, they must form in parallel from N, on independent pathways. It is interesting that the loss of very different elements of secondary structure can destabilize a protein to very similar extents.

AUTHOR CONTRIBUTIONS

Suman Pal: Conceptualization; formal analysis; investigation; methodology; software; validation; writing – original draft. **Jayant B. Udgaonkar:** Conceptualization; funding acquisition; resources; supervision; validation; visualization; writing – review and editing.

ACKNOWLEDGEMENTS

We thank members of our laboratory for discussions, and Dr. Santosh Jha and Dr. Jogender Singh for their comments on the manuscript. This work was funded by the Indian Institute of Science Education and Research Pune, by the Tata Institute of Fundamental Research, and a grant from the Department of Biotechnology [Grant number: BT/PR13369/COE/34/25/2015] Government of India. JBU is a recipient of a JC Bose National Fellowship from the Government of India.

All experiments were conducted in compliance with the ARRIVE guidelines.

CONFLICT OF INTEREST STATEMENT

The authors declare that they have no known competing financial interests or personal relationships that could have appeared to influence the work reported in this paper.

DATA AVAILABILITY STATEMENT

Data are available in the article's supplementary material.

ORCID

Suman Pal  <https://orcid.org/0009-0003-0873-9838>

REFERENCES

- Agashe, V. R., & Udgaonkar, J. B. (1995). Thermodynamics of denaturation of barstar: Evidence for cold denaturation and evaluation of the interaction with guanidine hydrochloride. *Biochemistry*, 34(10), 3286–3299.
- Bai, Y., Milne, J. S., Mayne, L., & Englander, S. W. (1993). Primary structure effects on peptide group hydrogen exchange. *Proceedings of the National Academy of Sciences*, 17(1), 75–86.



- Baiardi, S., Rossi, M., Capellari, S., & Parchi, P. J. B. P. (2019). Recent advances in the histo-molecular pathology of human prion disease. *Brain Pathology*, 29(2), 278–300.
- Bartz, J. C., McKenzie, D. I., Bessen, R. A., Marsh, R. F., & Aiken, J. M. (1994). Transmissible mink encephalopathy species barrier effect between ferret and mink: PrP gene and protein analysis. *Journal of General Virology*, 75(11), 2947–2953.
- Bernardi, L., & Bruni, A. C. (2019). Mutations in prion protein gene: Pathogenic mechanisms in C-terminal vs. N-terminal domain, a review. *International Journal of Molecular Sciences*, 20(14), 3606.
- Bett, C., Fernández-Borges, N., Kurt, T. D., Lucero, M., Nilsson, K. P. R., Castilla, J., & Sigurdson, C. J. (2012). Structure of the β 2- α 2 loop and interspecies prion transmission. *The FASEB Journal*, 26(7), 2868–2876.
- Bhate, S. H., Udgaonkar, J. B., & Das, R. (2021). Destabilization of polar interactions in the prion protein triggers misfolding and oligomerization. *Protein Science*, 30(11), 2258–2271.
- Biljan, I., Ilc, G., Giachin, G., Raspadori, A., Zhukov, I., Plavec, J., & Legname, G. (2011). Toward the molecular basis of inherited prion diseases: NMR structure of the human prion protein with V210I mutation. *Journal of Molecular Biology*, 412(4), 660–673.
- Biljan, I., Ilc, G., & Plavec, J. (2017). Analysis of prion protein structure using nuclear magnetic resonance spectroscopy. *Methods in Molecular Biology*, 1658, 35–49.
- Borchelt, D., Taraboulos, A., & Prusiner, S. (1992). Evidence for synthesis of scrapie prion proteins in the endocytic pathway. *Journal of Biological Chemistry*, 267(23), 16188–16199.
- Brown, D. R. (2006). Original article neurodegeneration and oxidative stress: Prion disease results from loss of antioxidant defence. *Folia Neuropathologica*, 43(4), 229–243.
- Büeler, H., Fischer, M., Lang, Y., Bluethmann, H., Lipp, H.-P., DeArmond, S. J., Prusiner, S. B., Aguet, M., & Weissmann, C. (1992). Normal development and behaviour of mice lacking the neuronal cell-surface PrP protein. *Nature*, 356(6370), 577–582.
- Burns, C. S., Aronoff-Spencer, E., Dunham, C. M., Lario, P., Avdievich, N. I., Antholine, W. E., Olmstead, M. M., Vrieling, A., Gerfen, G. J., & Peisach, J. (2002). Molecular features of the copper binding sites in the octarepeat domain of the prion protein. *Biochemistry*, 41(12), 3991–4001.
- Caldarulo, E., Barducci, A., Wüthrich, K., & Parrinello, M. (2017). Prion protein β 2- α 2 loop conformational landscape. *Proceedings of the National Academy of Sciences*, 114(36), 9617–9622.
- Caughy, B., Baron, G. S., Chesebro, B., & Jeffrey, M. (2009). Getting a grip on prions: Oligomers, amyloids, and pathological membrane interactions. *Annual Review of Biochemistry*, 78, 177–204.
- Chich, J.-F., Chapuis, C., Henry, C., Vidic, J., Rezaei, H., & Noinville, S. (2010). Vesicle permeabilization by purified soluble oligomers of prion protein: A comparative study of the interaction of oligomers and monomers with lipid membranes. *Journal of Molecular Biology*, 397(4), 1017–1030.
- Choi, C. J., Anantharam, V., Saetveit, N. J., Houk, R. S., Kanthasamy, A., & Kanthasamy, A. G. (2007). Normal cellular prion protein protects against manganese-induced oxidative stress and apoptotic cell death. *Toxicological Sciences*, 98(2), 495–509.
- Coleman, B. M., Harrison, C. F., Guo, B., Masters, C. L., Barnham, K. J., Lawson, V. A., & Hill, A. F. (2014). Pathogenic mutations within the hydrophobic domain of the prion protein lead to the formation of protease-sensitive prion species with increased lethality. *Journal of Virology*, 88(5), 2690–2703.
- Collinge, J., Whittington, M. A., Sidle, K. C., Smith, C. J., Palmer, M. S., Clarke, A. R., & Jefferys, J. G. (1994). Prion protein is necessary for normal synaptic function. *Nature*, 370(6487), 295–297.
- Dima, R. I., & Thirumalai, D. (2004). Probing the instabilities in the dynamics of helical fragments from mouse PrP. *Proceedings of the National Academy of Sciences*, 101(43), 15335–15340.
- Eaton, W. A., & Wolynes, P. G. (2017). Theory, simulations, and experiments show that proteins fold by multiple pathways. *Proceedings of the National Academy of Sciences*, 114(46), E9759–E9760.
- Erlich, P., Dumestre-Pérard, C., Ling, W. L., Lemaire-Vieille, C., Schoehn, G., Arlaud, G. J., Thielens, N. M., Gagnon, J., & Cesbron, J.-Y. (2010). Complement protein C1q forms a complex with cytotoxic prion protein oligomers. *Journal of Biological Chemistry*, 285(25), 19267–19276.
- Gasperini, L., & Legname, G. (2014). Prion protein and aging. *Frontiers in Cell and Developmental Biology*, 2, 44.
- Giachin, G., Ilc, G., Biljan, I., Jaremko, M., Jaremko, L., Benetti, F., Plavec, J., Zhukov, I., & Legname, G. (2011). In NMR structure of the human prion protein with the pathological Q212P mutation: Insights into inherited human prion diseases. Bio-NMR and EAST-NMR Annual User Meeting.
- Goluguri, R. R., Sen, S., & Udgaonkar, J. (2019). Microsecond sub-domain motions and the folding and misfolding of the mouse prion protein. *eLife*, 8, e44766.
- Hadži, S., Ondračka, A., Jerala, R., & Hafner-Bratkovič, I. (2015). Pathological mutations H187R and E196K facilitate subdomain separation and prion protein conversion by destabilization of the native structure. *The FASEB Journal*, 29(3), 882–893.
- Haigh, C. L., Marom, S. Y., & Collins, S. J. (2010). Copper, endoproteolytic processing of the prion protein and cell signalling. *Frontiers in Bioscience-Landmark*, 15(3), 1086–1104.
- Hegde, R. S., Mastrianni, J. A., Scott, M. R., DeFea, K. A., Tremblay, P., Torchia, M., DeArmond, S. J., Prusiner, S. B., & Lingappa, V. R. (1998). A transmembrane form of the prion protein in neurodegenerative disease. *Science*, 279(5352), 827–834.
- Hu, W., Kan, Z.-Y., Mayne, L., & Englander, S. W. (2016). Cytochrome c folds through foldon-dependent native-like intermediates in an ordered pathway. *Proceedings of the National Academy of Sciences*, 113(14), 3809–3814.
- Hu, W., Walters, B. T., Kan, Z.-Y., Mayne, L., Rosen, L. E., Marqusee, S., & Englander, S. W. (2013). Stepwise protein folding at near amino acid resolution by hydrogen exchange and mass spectrometry. *Proceedings of the National Academy of Sciences*, 110(19), 7684–7689.
- Huang, D., & Caflish, A. (2015). Evolutionary conserved Tyr169 stabilizes the β 2- α 2 loop of the prion protein. *Journal of the American Chemical Society*, 137(8), 2948–2957.
- Huang, L., Jin, R., Li, J., Luo, K., Huang, T., Wu, D., Wang, W., Chen, R., & Xiao, G. (2010). Macromolecular crowding converts the human recombinant PrP^C to the soluble neurotoxic β -oligomers. *The FASEB Journal*, 24(9), 3536–3543.
- Hughson, F. M., Wright, P. E., & Baldwin, R. L. (1990). Structural characterization of a partly folded apomyoglobin intermediate. *Science*, 249(4976), 1544–1548.
- Jackson, S. E., Moracci, M., elMasry, N., Johnson, C. M., & Fersht, A. R. (1993). Effect of cavity-creating mutations in the hydrophobic core of chymotrypsin inhibitor 2. *Biochemistry*, 32(42), 11259–11269.
- Jain, S., & Udgaonkar, J. B. (2008). Evidence for stepwise formation of amyloid fibrils by the mouse prion protein. *Journal of Molecular Biology*, 382(5), 1228–1241.
- Jung Cheng, C., & Daggett, V. (2014). Different misfolding mechanisms converge on common conformational changes: Human prion protein pathogenic mutants Y218N and E196K. *Prion*, 8(1), 125–135.
- Kamatari, Y. O., Hayano, Y., Yamaguchi, K. i., Hosokawa-Muto, J., & Kuwata, K. (2013). Characterizing anti-prion compounds based on their binding properties to prion proteins: Implications as medical chaperones. *Protein Science*, 22(1), 22–34.
- Khan, M. Q., Sweeting, B., Mulligan, V. K., Arslan, P. E., Cashman, N. R., Pai, E. F., & Chakrabarty, A. (2010). Prion disease susceptibility is affected by β -structure folding propensity and local side-chain interactions in PrP. *Proceedings of the National Academy of Sciences*, 107(46), 19808–19813.

- Kretzschmar, H., Prusiner, S., Stowring, L., & DeArmond, S. (1986). Scrapie prion proteins are synthesized in neurons. *The American Journal of Pathology*, 122(1), 1–5.
- Kurt, T. D., Bett, C., Fernández-Borges, N., Joshi-Barr, S., Hornemann, S., Rüllicke, T., Castilla, J., Wüthrich, K., Aguzzi, A., & Sigurdson, C. J. (2014). Prion transmission prevented by modifying the $\beta 2$ - $\alpha 2$ loop structure of host PrP. *Journal of Neuroscience*, 34(3), 1022–1027.
- Kurt, T. D., Jiang, L., Bett, C., Eisenberg, D., & Sigurdson, C. J. (2014). A proposed mechanism for the promotion of prion conversion involving a strictly conserved tyrosine residue in the $\beta 2$ - $\alpha 2$ loop of PrP. *Journal of Biological Chemistry*, 289(15), 10660–10667.
- Kuwata, K., Nishida, N., Matsumoto, T., Kamatari, Y. O., Hosokawa-Muto, J., Kodama, K., Nakamura, H. K., Kimura, K., Kawasaki, M., & Takakura, Y. (2007). Hot spots in prion protein for pathogenic conversion. *Proceedings of the National Academy of Sciences*, 104(29), 11921–11926.
- Legname, G. (2017). Elucidating the function of the prion protein. *PLoS Pathogens*, 13(8), e1006458.
- Málaga-Trillo, E., Solis, G. P., Schrock, Y., Geiss, C., Lunz, L., Thomanetz, V., & Stuermer, C. A. O. (2009). Regulation of embryonic cell adhesion by the prion protein. *PLoS Biology*, 7(3), e1000055.
- Martins, V. R., Linden, R., Prado, M. A., Walz, R., Sakamoto, A. C., Izquierdo, I., & Brentani, R. R. (2002). Cellular prion protein: On the road for functions. *FEBS Letters*, 512(1–3), 25–28.
- Meli, M., Gasset, M., & Colombo, G. (2011). Dynamic diagnosis of familial prion diseases supports the $\beta 2$ - $\alpha 2$ loop as a universal interference target. *PLoS One*, 6(4), e19093.
- Milhavet, O., & Lehmann, S. (2002). Oxidative stress and the prion protein in transmissible spongiform encephalopathies. *Brain Research Reviews*, 38(3), 328–339.
- Moore, R. A., Herzog, C., Errett, J., Kocisko, D. A., Arnold, K. M., Hayes, S. F., & Priola, S. A. (2006). Octapeptide repeat insertions increase the rate of protease-resistant prion protein formation. *Protein Science*, 15(3), 609–619.
- Moore, R. A., Taubner, L. M., & Priola, S. A. (2009). Prion protein misfolding and disease. *Journal of Current Opinion in Structural Biology*, 19(1), 14–22.
- Moulick, R., Das, R., & Udgaonkar, J. B. (2015). Partially unfolded forms of the prion protein populated under misfolding-promoting conditions: Characterization by hydrogen exchange mass spectrometry and NMR. *Journal of Biological Chemistry*, 290(42), 25227–25240.
- Moulick, R., Goluguri, R. R., & Udgaonkar, J. B. (2019). Ruggedness in the free energy landscape dictates misfolding of the prion protein. *Journal of Molecular Biology*, 431(4), 807–824.
- Moulick, R., & Udgaonkar, J. B. (2017). Identification and structural characterization of the precursor conformation of the prion protein which directly initiates misfolding and oligomerization. *Journal of Molecular Biology*, 429(6), 886–899.
- Nguyen, D., Mayne, L., Phillips, M. C., & Walter Englander, S. (2018). Reference parameters for protein hydrogen exchange rates. *Journal of the American Society for Mass Spectrometry*, 29(9), 1936–1939.
- Ning, L., Guo, J., Jin, N., Liu, H., & Yao, X. (2014). The role of Cys179–Cys214 disulfide bond in the stability and folding of prion protein: Insights from molecular dynamics simulations. *Journal of Molecular Modeling*, 20, 1–8.
- Pal, S., & Udgaonkar, J. B. (2022). Evolutionarily conserved proline residues impede the misfolding of the mouse prion protein by destabilizing an aggregation-competent partially unfolded form. *Journal of Molecular Biology*, 434(23), 167854.
- Park, C., & Marqusee, S. (2004). Probing the high energy states in proteins by proteolysis. *Journal of Molecular Biology*, 343(5), 1467–1476.
- Prigent, S., & Rezaei, H. (2011). PrP assemblies: Spotting the responsible regions in prion propagation. *Prion*, 5(2), 69–75.
- Rana, A., Gnanewari, D., Bansal, S., & Kundu, B. (2009). Prion metal interaction: Is prion pathogenesis a cause or a consequence of metal imbalance? *Chemico-Biological Interactions*, 181(3), 282–291.
- Riek, R., Hornemann, S., Wider, G., Billeter, M., Glockshuber, R., & Wüthrich, K. (1996). NMR structure of the mouse prion protein domain PrP (121–231). *Nature*, 382, 180–182.
- Sabareesan, A., & Udgaonkar, J. B. (2016). Pathogenic mutations within the disordered palindromic region of the prion protein induce structure therein and accelerate the formation of misfolded oligomers. *Journal of Molecular Biology*, 428(20), 3935–3947.
- Schmitt-Ulms, G., Legname, G., Baldwin, M. A., Ball, H. L., Bradon, N., Bosque, P. J., Crossin, K. L., Edelman, G. M., DeArmond, S. J., & Cohen, F. E. (2001). Binding of neural cell adhesion molecules (N-CAMs) to the cellular prion protein. *Journal of Molecular Biology*, 314(5), 1209–1225.
- Scialò, C., De Cecco, E., Manganotti, P., & Legname, G. (2019). Prion and prion-like protein strains: Deciphering the molecular basis of heterogeneity in neurodegeneration. *Biochemical Journal*, 11(3), 261.
- Sengupta, I., Bhate, S. H., Das, R., & Udgaonkar, J. B. (2017). Salt-mediated oligomerization of the mouse prion protein monitored by real-time NMR. *Journal of Molecular Biology*, 429(12), 1852–1872.
- Sengupta, I., & Udgaonkar, J. (2019). Monitoring site-specific conformational changes in real-time reveals a misfolding mechanism of the prion protein. *eLife*, 8, e44698.
- Sigurdson, C. J., Joshi-Barr, S., Bett, C., Winson, O., Manco, G., Schwarz, P., Rüllicke, T., Nilsson, K. P. R., Margalith, I., & Raeber, A. (2011). Spongiform encephalopathy in transgenic mice expressing a point mutation in the $\beta 2$ - $\alpha 2$ loop of the prion protein. *Journal of Neuroscience*, 31(39), 13840–13847.
- Simoneau, S., Rezaei, H., Salès, N., Kaiser-Schulz, G., Lefebvre-Roque, M., Vidal, C., Fournier, J.-G., Comte, J., Wopfner, F., & Grosclaude, J. (2007). In vitro and in vivo neurotoxicity of prion protein oligomers. *PLoS Pathogens*, 3(8), e125.
- Singh, J., Kumar, H., Sabareesan, A. T., & Udgaonkar, J. B. (2014). Rational stabilization of helix 2 of the prion protein prevents its misfolding and oligomerization. *Journal of the American Chemical Society*, 136(48), 16704–16707.
- Singh, J., & Udgaonkar, J. B. (2015). Structural effects of multiple pathogenic mutations suggest a model for the initiation of misfolding of the prion protein. *Angewandte Chemie*, 127(26), 7639–7643.
- Singh, J., & Udgaonkar, J. B. (2016a). Unraveling the molecular mechanism of pH-induced misfolding and oligomerization of the prion protein. *Journal of Molecular Biology*, 428(6), 1345–1355.
- Singh, J., & Udgaonkar, J. B. (2016b). The pathogenic mutation T182A converts the prion protein into a molten globule-like conformation whose misfolding to oligomers but not to fibrils is drastically accelerated. *Biochemistry*, 55(3), 459–469.
- Slapšak, U. k., Salzano, G., Ilc, G., Giachin, G., Bian, J., Telling, G., Legname, G., & Plavec, J. (2019). Unique structural features of mule deer prion protein provide insights into chronic wasting disease. *ACS Omega*, 4(22), 19913–19924.
- Steele, A. D., Lindquist, S., & Aguzzi, A. (2007). The prion protein knock-out mouse: A phenotype under challenge. *Prion*, 1(2), 83–93.
- Van der Kamp, M. W., & Daggett, V. (2010). Influence of pH on the human prion protein: Insights into the early steps of misfolding. *Biophysical Journal*, 99(7), 2289–2298.
- van Rheede, T., Smolenaars, M. M., Madsen, O., & de Jong, W. W. (2003). Molecular evolution of the mammalian prion protein. *Molecular Biology and Evolution*, 20(1), 111–121.
- Vanni, I., Pirisinu, L., Acevedo-Morantes, C., Kamali-Jamil, R., Rathod, V., Di Bari, M. A., D'Agostino, C., Marcon, S., Esposito, E., & Riccardi, G. (2020). Isolation of infectious, non-fibrillar and oligomeric prions from a genetic prion disease. *Brain*, 143(5), 1512–1524.
- Vassallo, N., & Herms, J. (2003). Cellular prion protein function in copper homeostasis and redox signalling at the synapse. *Journal of Neurochemistry*, 86(3), 538–544.

- Watt, N. T., & Hooper, N. M. (2003). The prion protein and neuronal zinc homeostasis. *Trends in Biochemical Sciences*, 28(8), 406–410.
- Wedemeyer, W. J., Welker, E., & Scheraga, H. A. (2002). Proline cis-trans isomerization and protein folding. *Biochemistry*, 41(50), 14637–14644.
- Wong, B. S., Liu, T., Li, R., Pan, T., Petersen, R. B., Smith, M. A., Gambetti, P., Perry, G., Manson, J. C., & Brown, D. R. (2001). Increased levels of oxidative stress markers detected in the brains of mice devoid of prion protein. *Journal of Neurochemistry*, 76(2), 565–572.
- Wrabl, J., & Shortle, D. (1999). A model of the changes in denatured state structure underlying m value effects in staphylococcal nuclease. *Nature Structural Biology*, 6(9), 876–883.
- Yu, H., Liu, X., Neupane, K., Gupta, A. N., Brigley, A. M., Solanki, A., Sosova, I., & Woodside, M. T. (2012). Direct observation of multiple misfolding pathways in a single prion protein molecule. *Proceedings of the National Academy of Sciences*, 109(14), 5283–5288.
- Zhang, J. (2011). Comparison studies of the structural stability of rabbit prion protein with human and mouse prion proteins. *Journal of Theoretical Biology*, 269(1), 88–95.

Zhang, J. (2015). A survey on π - π stackings and π -cations in prion protein structures: A 'quick reference card'. *Biochemical Pharmacology*, 4(3), e175.

SUPPORTING INFORMATION

Additional supporting information can be found online in the Supporting Information section at the end of this article.

How to cite this article: Pal, S., & Udgaonkar, J. B. (2023). Mutations of evolutionarily conserved aromatic residues suggest that misfolding of the mouse prion protein may commence in multiple ways. *Journal of Neurochemistry*, 00, 1–15. <https://doi.org/10.1111/jnc.16007>